Kinetics study of the evolution of oxygen-related defects in mono-crystalline silicon subjected to electron-irradiation and thermal treatment

V. Quemener,[1,a)] B. Raeissi,[1] F. Herklotz,[1] L. I. Murin,[2] E. V. Monakhov,[1] and B. G. Svensson[1]
[1]*Department of Physics/Center for Materials Science and Nanotechnology, University of Oslo, P.O. Box 1048 Blindern, N-0316 Oslo, Norway*
[2]*Scientific-Practical Materials Research Center of NAS of Belarus, Minsk 220072, Belarus*

(Received 3 August 2015; accepted 17 September 2015; published online 2 October 2015)

The diffusion and dissociation mechanisms governing the evolution of oxygen and vacancy-oxygen defects in Czochralski-grown Si samples have been studied. The samples were irradiated at (i) room temperature or (ii) elevated temperature (350 °C) by MeV electrons and then isothermally annealed at 8 different temperatures in the range of 300 °C to 500 °C. The evolution of the concentrations of oxygen complexes (O_n, $n \leq 3$) and mono-vacancy-oxygen defects (VO_n, $n \leq 4$) have been followed by infrared absorption measurements of local vibrational modes originating from the individual defects. The experimental kinetics data have been compared with simulation results based on the theory for diffusion limited reactions, assuming a model where sequential build-up of the VO_n defects is a key ingredient. A close quantitative agreement is obtained for both sets of samples despite quite different initial conditions prior to the annealing, which adds evidence to the validity of the model. Values for the diffusivity and dissociation rates of VO_n ($n \leq 4$) and O_n ($n \leq 3$) have been deduced and in general, the mobility and stability of VO_n decrease and increase with n, respectively. For all the defects, partial dissociation appears as a prevailing process during diffusion, while full dissociation of VO_n is limited by an energy barrier identical to that of interstitial oxygen (O_i) diffusion (~2.55 eV). The oxygen dimer and trimer are fast diffusers but slower than substitutional oxygen, i.e., VO; VO is found to be the most mobile species, whilst O_i is the slowest one with a difference in diffusivity of up to 7 orders of magnitude in the studied temperature range.
 [http://dx.doi.org/10.1063/1.4932019]

I. INTRODUCTION

Oxygen is one of the most important and most studied impurities in solar-grade silicon. Although interstitial oxygen atoms (O_i) are electrically neutral, rather stable and immobile at room temperature, they strongly contribute to and influence major defects in silicon during crystallization and high temperature processing. For instance, oxygen precipitates, thermal donors, and defects causing light induced degradation are all related to oxygen and affect the performance of photovoltaic cells.[1–4] In particular, the comprehension of oxygen diffusion is crucial to predict defect evolution in mono-crystalline silicon; for instance, oxygen aggregation occurs with a much lower activation energy (1.8 eV) than that of interstitial oxygen diffusion (2.53 eV). Accordingly, a fast diffusing oxygen containing species is required in order to explain the aggregation, and oxygen complexes (O_n) and vacancy-oxygen defects (VO_n) (n is an integer ≥ 1)[5–8] are considered as potential candidates. Some of these defects are indeed shown to exhibit a higher diffusivity than O_i, indicating that they may play a role in the formation of thermal donors and oxygen precipitates.[9–13] Thus, a deep and quantitative understanding of the diffusion and dissociation mechanisms governing the evolution of VO_n and O_n defects is crucial in order to control their impact. One of the most suitable methods for studying oxygen-containing defects in silicon is local vibrational mode (LVM) spectroscopy. In particular, Fourier-transform infrared spectroscopy (FTIR) has been exploited to identify oxygen dimers,[9,11] trimers,[14] and a number of vacancy-oxygen complexes. So far, mainly VO and VO_2 centers have been quantitatively studied and some key information about their diffusion/dissociation mechanisms has been obtained.[11,15–17] However, data for the larger VO_n defects ($n = 3, 4$) are scarce in the literature. Most recently, LVMs associated to VO_3 and VO_4 have been identified, which enables investigations of their diffusion and dissociation properties in detail.[7,18,19] In addition, Quemener *et al.*[20] have reported initial data on the formation and annealing kinetics of VO_n defects and compared the experimental results with a model assuming sequential reactions of $VO_n + O_i \rightarrow VO_{n+1}$, ($n \geq 1$). However, in this initial study, the role of O_n complexes and their interplay with VO_n defects was not included.

In the present work, a comprehensive study has been undertaken to unveil the processes governing the evolution of O_n and VO_n defects during isothermal treatment at eight different temperatures in the range of 300 °C to 500 °C. Two independent sets of Czochralski-grown (Cz) samples have been investigated, one irradiated with MeV electrons at room temperature (RT) and one irradiated at elevated temperature yielding drastically different initial concentrations of the O_n and VO_n defects prior to the thermal treatment, i.e., defects with $n \leq 2$ are strongly promoted by the irradiation at

a)Electronic mail: vincent.quemener@smn.uio.no

elevated temperature, as previously shown in some detail by Lindström *et al.*[18] However, the experimental data for both sets of samples, as obtained by LVM spectroscopy, are demonstrated to be accurately described by the same defect reactions model and the same values for diffusivities and dissociation rates of the different O_n and VO_n defects, providing evidence for the general validity of the model. In general, the diffusivity is found to decrease with increasing n and the same holds also for the dissociation rate. There are, however, two exceptions from this trend: (i) O_i is the species with the lowest diffusivity and (ii) O_3 (the oxygen trimer) exhibits a high dissociation rate as may be expected from its anticipated atomic configuration.

II. EXPERIMENT

The samples used were cut from Cz-Si phosphorus doped wafers having a resistivity of 10–50 Ω cm and with concentrations of O_i and substitutional carbon (C_s) of $(1–1.3)\times10^{18}\,cm^{-3}$ and $\leq5\times10^{15}\,cm^{-3}$, respectively. Two sets of the samples were irradiated with 2.5 MeV electrons at RT and at 350 °C (hot irradiation), respectively, with fluences in the range of $(1–40)\times10^{17}\,cm^{-2}$ and a flux of $\sim3\times10^{13}\,cm^{-2}s^{-1}$. After irradiation, the samples were isothermally annealed in a tube furnace with nitrogen flow at 300, 350, 370, 400, 425, 450, 470, and 500 °C. After each annealing stage, the concentrations of O_n and VO_n defects were determined by FTIR measurements using a Bruker IFS 113v and/or a Bruker IFS 125HR Fourier-transform IR spectrometer with the samples kept at RT and a spectral resolution of $1\,cm^{-1}$.

The defect concentrations were deduced from the peak amplitudes of the associated LVM absorption bands: for O_i ($1107\,cm^{-1}$), O_2 (1013, $1062\,cm^{-1}$), VO ($830\,cm^{-1}$), VO_2 ($888.5\,cm^{-1}$), VO_3 (905, $969\,cm^{-1}$), and VO_4 ($985\,cm^{-1}$), with calibration coefficients of 3.14×10^{17}, 7.2×10^{16}, 8.5×10^{16}, 4.25×10^{16}, 8.5×10^{16}, and $4.25\times10^{16}\,cm^{-2}$, respectively.[19,21] The peak amplitudes have been used for the quantification and not the integrated peak area, because the calibration coefficients are known for the peak amplitudes. Further, the use of peak amplitudes minimizes the overlap between different defects when deducing concentration values. A relative error of ≤10% is estimated for the concentration of the different defects.

III. RESULTS AND DISCUSSIONS

A. Absorption spectra

Figure 1 shows the absorption spectra of samples irradiated at RT (a) and at 350 °C (b) and subsequently annealed at 370 °C for different durations. A large difference is found between the defects present in Figs. 1(a) and 1(b) after irradiation and no annealing. In Fig. 1(a), only VO appears but after the annealing a successive formation of VO_2, VO_3, and VO_4 take place, which can be described via the sequential reactions $VO_n + O_i \rightarrow VO_{n+1}$, $(n \geq 1)$.[20] In the case of hot irradiation (Fig. 1(b)), VO is also present initially but with a low concentration while especially VO_2 but also VO_3 and VO_4 are more dominant; the high concentration of VO_2 is attributed to mobile VO's reacting with O_i as the main trap. In addition, interstitial Si atoms (I_{Si}) generated during the irradiation can be trapped by VO_2 forming O_2 complexes via the reaction $VO_2 + I_{Si} \rightarrow O_2$, as evidenced by the pronounced O_2 LVM having a similar peak intensity as that of the VO_2 peak. Moreover, the oxygen dimer O_2 is known to be a fast diffusing species[10,11,22] and can contribute to the formation of VO_n complexes through the reactions $VO_n + O_2 \rightarrow VO_{n+2}$, $(n \geq 1)$. Here, it can also be noted that O_2 is present already in the as-grown material with a significant concentration but exhibits no increase after the RT irradiation (Fig. 1(a)). This is attributed to the lack of VO_2 formation during the RT irradiation (because of the low mobility of VO at RT) and in direct contrast to that during the 350 °C irradiations, the reaction $VO_2 + I_{Si} \rightarrow O_2$ does not take place.[18] The evolution of the different defects as a function of annealing time and annealing temperature will be discussed in Section III C.

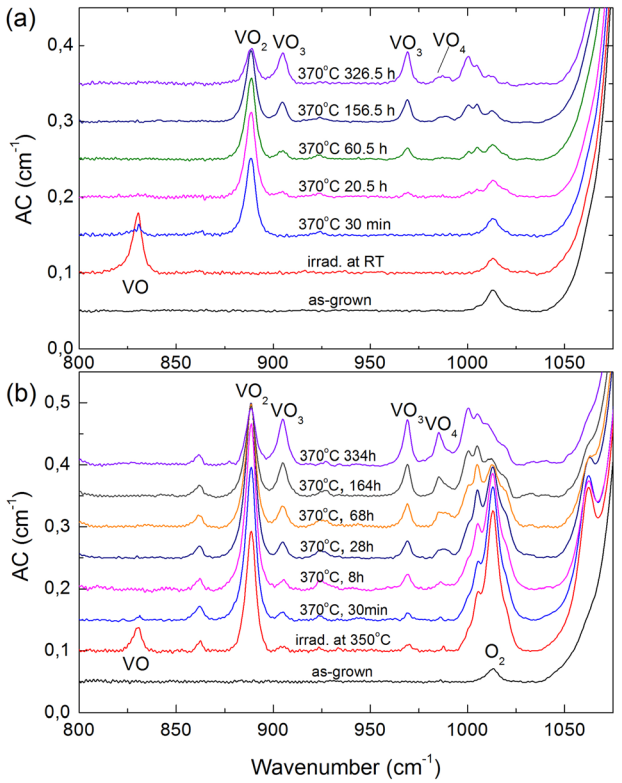

FIG. 1. Section of absorption spectra measured at room temperature after RT irradiation (a) and hot irradiation (b) and subsequent isothermal annealing at 370 °C for different times up to 334 h.

B. Kinetics model

The experimentally observed defect evolution is modeled within the framework of the theory of diffusion-limited reactions,[23] assuming a sequential build-up of the oxygen and vacancy-oxygen defects with diffusion/dissociation reactions as core ingredients. A reaction occurs between two species when they migrate and agglomerate into a larger one after approaching each other within a capture radius R. The reaction rate is given by $4\pi R(D_A + D_B)[A][B]$, where D_A and D_B represent the diffusion constants and [A] and [B] are

the concentrations of the two species A and B, respectively. R has been treated as a temperature independent constant and put equal to a geometrical value of 5 Å. An alternative value of R = 10 Å affects mainly the pre-exponential factor of the diffusion constants through a lowering by a factor of two and is found to have minor (if any) effect on the agreement between the experimental and modeling results. A back reaction occurs when a defect dissociates into smaller species, and the dissociation rate is given by $K_C[C]$, where K_C represents the rate constant and [C] is the concentration of the species C. The diffusion and dissociation constants are given by the relations $D = d_0 \exp(-E_a^{migration}/kT)$ and $K = k_0 \exp(-E_a^{dissociation}/kT)$, respectively, where d_0 and k_0 are the exponential prefactors, $E_a^{migration}$ and $E_a^{dissociation}$ are the activation energies, k is the Boltzmann constant, and T is the absolute temperature.

Sections III B 1 and III B 2 describe the development of the simulation model with reactions included for the VO_n defects and the O_n defects, respectively. The possible role of divacancy centers on the evolution of the VO_n and O_n defects has been omitted in the model because of their low introduction rate relative to the VO centers in irradiated Cz material and their limited thermal stability (see Ref. 24 and references therein).

1. Reactions of vacancy–oxygen (VO_n) defects

The sum of the four VO_n species monitored experimentally reveals the evolution of the total vacancy concentration in the system during the annealing treatments. Figure 2 shows the total concentration of vacancies $[V] = [VO] + [VO_2] + [VO_3] + [VO_4]$ versus annealing time for both the RT-irradiated and the hot-irradiated samples treated at temperatures between 370 °C and 470 °C. For the RT-irradiated ones annealed at 370 °C and 400 °C, [V] remains constant up to the maximum annealing duration employed, implying that the formation of VO_n ($n \geq 2$) arises from VO only and no (or negligible) loss/generation of V's to/from other processes

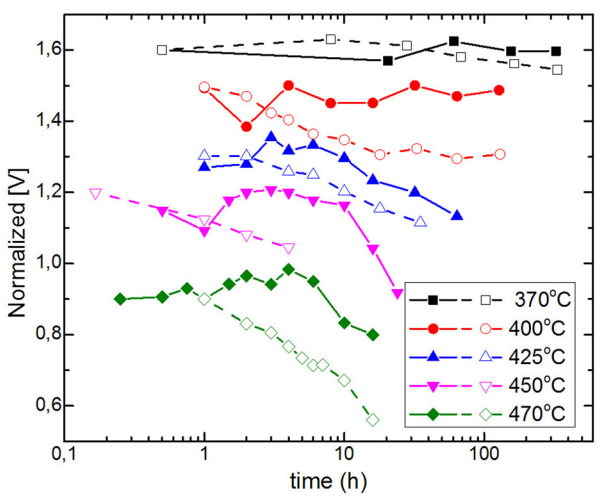

FIG. 2. Sum of the VO, VO_2, VO_3, and VO_4 species for RT irradiated (solid symbols) and hot irradiated (open symbols) samples versus time during isothermal annealing at different temperatures. The values are normalized with respect to the initial one (after irradiation and no annealing), and for clarity, the curves are displaced along the ordinate.

occurs. At higher temperatures, the general trend is a slight decrease of [V] with time, indicating that VO_4 is not the "final" defect and larger cluster (VO_n with $n > 4$) are formed and/or that VO_4 dissociates into other defects with a loss of V's. For the hot-irradiated samples, a somewhat more pronounced decrease of [V] occurs with increasing temperature, consistent with that VO_4 is not the "final" defect and also indicating that O_2 plays a role in the evolution of the VO_n species, i.e., reactions such as $VO_3 + O_2 \rightarrow VO_5$ and $VO_4 + O_2 \rightarrow VO_6$ are important to take into account.[19] Moreover, $[O_2]$ displays a clear decrease with annealing time (as depicted in Figs. 4–6), which cannot be accounted for by the increase of $[VO_n]$ ($n \geq 3$) corroborating that O_2 is a diffusing and reactive species that contributes to the formation of other complexes than the VO_n defects.

On the basis of the considerations given above, the following reactions (1a)–(1h) of VO_n with O_i and O_2 are included in the simulation model used:

$$VO + O_i \rightarrow VO_2, \quad (1a)$$

$$VO + O_2 \rightarrow VO_3, \quad (1b)$$

$$VO_2 + O_i \rightarrow VO_3, \quad (1c)$$

$$VO_2 + O_2 \rightarrow VO_4, \quad (1d)$$

$$VO_3 + O_i \rightarrow VO_4, \quad (1e)$$

$$VO_3 + O_2 \rightarrow VO_5, \quad (1f)$$

$$VO_4 + O_i \rightarrow VO_5, \quad (1g)$$

$$VO_4 + O_2 \rightarrow VO_6. \quad (1h)$$

As previously discussed in the literature, the VO_n defects can break up during annealing.[15,16] Although it is obvious that VO can only dissociate into V and O_i, the higher order species may dissociate by different mechanisms. For instance, VO_2 may dissociate into $VO + O_i$ and/or $V + O_2$. However, the atomic configuration of VO_2 is two oxygen atoms sharing a single vacancy where the O–O interaction is weak (or even non-existent), as found both experimentally[25] and theoretically.[26] That is, VO_2 is not a monovacancy accommodating an O_2 dimer, which is also substantiated by the metastable configuration of VO_2, labeled VO_2^*.[27] In VO_2^*, one of the two O atoms is situated just outside the vacancy as an O_i in a neighboring bond. Hence, the dissociation of VO_2 into $VO + O_i$ is considered to be the prevailing mechanism. It is also evident that the dissociation of VO_3 will follow a similar process, since the atomic structure of VO_3 resembles that of $VO_2 + Oi$,[6] i.e., $VO_3 \rightarrow VO_2 + O_i$. Further, VO_4 is assumed to be immobile, and the reactions $VO_4 + O_i \rightarrow VO_5$ and $VO_4 + O_2 \rightarrow VO_6$ are governed by the diffusion of O_i and O_2, respectively. However, these reactions are not sufficient to explain the observed evolution of $[VO_4]$ with time and temperature, and hence, also dissociation of VO_4 into $V + O_4$ is considered. Other dissociation mechanisms of VO_4 have also been evaluated, such as $VO_4 \rightarrow VO_2 + O_2$ and $VO_4 \rightarrow VO_3 + O_i$, but they tend to give steady-state concentrations of VO_2 and VO_3 after long annealing times which contradict the experimental results. Finally, at the highest annealing temperatures

studied (e.g., 500 °C), VO_3 and VO_4 remain with substantial concentrations after long duration suggesting dissociation of VO_5 and VO_6 into VO_3 and VO_4. Accordingly, the following dissociative reactions (2a)–(2g) of the VO_n defects are included in the model:

$$VO \rightarrow V + O_i, \tag{2a}$$

$$VO_2 \rightarrow VO + O_i, \tag{2b}$$

$$VO_3 \rightarrow VO_2 + O_i, \tag{2c}$$

$$VO_4 \rightarrow V + O_4, \tag{2d}$$

$$VO_5 \rightarrow VO_3 + O_2, \tag{2e}$$

$$VO_5 \rightarrow VO_4 + O_i, \tag{2f}$$

$$VO_6 \rightarrow VO_4 + O_2. \tag{2g}$$

Figure 3 displays the evolution of VO_2 in the two sets of irradiated samples versus time during isothermal annealing at 350 °C, 400 °C, and 425 °C. In Fig. 3(a), the solid line represents the simulation results using all the equations described above, and a close agreement with the experimental data is found. In particular, the VO_2 evolution is rather different at the three temperatures but still well described by the model with the reactions $VO + O_i \rightarrow VO_2$ and $VO_2 + O_i \rightarrow VO_3$ as the dominant ones initially and after long duration, respectively.

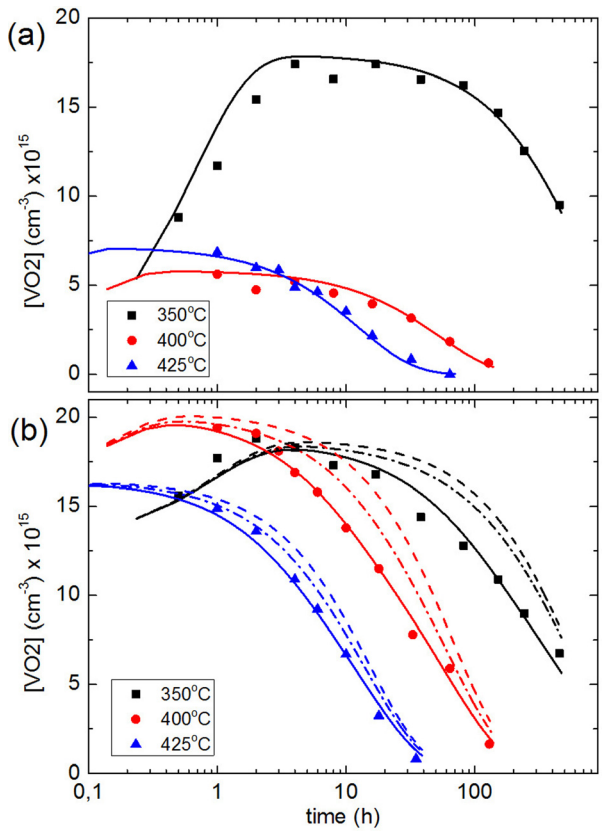

FIG. 3. Comparison between simulated (line) and experimental (symbols) concentrations of VO_2 for samples irradiated at RT (Fig. 3(a)) and at 350 °C (Fig. 3(b)) versus time during isothermal annealing at 350 °C, 400 °C, and 425 °C. For the hot-irradiated samples, three simulation curves are compared: (i) $[O_2]_{t=0} = 0$ (dashed line), (ii) $[O_2]_{t=0}$ equal to the experimental value of $[O_2]$ after irradiation (dashed dotted line), (iii) as for (ii) but with the addition of the defect A (solid line).

In Fig. 3(b), simulation results are shown for three different models. In the first case, $[O_2]_{t=0}$ is put equal to zero, similar to that for the RT-irradiated samples (Fig. 3(b), dashed line). However, the simulated data overestimate the experimental ones. If we initialize $[O_2]_{t=0}$ using the corresponding experimental one, a significant improvement takes place providing evidence for the influence of O_2 on the VO_2 evolution (Fig. 3(b), dashed dotted line). Despite the improvement, the agreement is still not satisfactory (with a possible exception for the 425 °C data) and this holds especially for $t \geq 2h$ at 350 and 400 °C. Until now, any role of Si self-interstitials (I_{Si}), which are generated in equal amount as the V's during the electron irradiation, has been omitted for the VO_n evolution. In particular, during the hot irradiation clusters of I's may be expected to form since the competition to trap I's by carbon is suppressed; C_s is a main trap for migrating I's at RT and prominent interstitial-carbon-related defects occur, like for example, interstitial carbon (C_i) and C_iO_i- and C_iC_s-pairs.[28] Several of these C_i-related defects do, however, not form at 350 °C because of a limited temperature stability enhancing the probability of generating more stable clusters of I_{Si}. On the basis of these arguments, a defect labelled A is introduced, which dissociates and releases I_{Si} interacting with VO_n via $I_{Si} + VO_n \rightarrow O_n$ ($n \geq 1$) (see Fig. 3(b), solid line). The value assumed for $[A]_{t=0}$ is small and only 10% of $[O_2]_{t=0}$ (in RT-irradiated samples $[A]_{t=0} = 0$) but the agreement with the measured data becomes now excellent. Accordingly, the following equations (3a)–(3e) have been included in our simulation model:

$$A \rightarrow I_{Si} + A', \tag{3a}$$

$$I_{Si} + VO \rightarrow O_i, \tag{3b}$$

$$I_{Si} + VO_2 \rightarrow O_2, \tag{3c}$$

$$I_{Si} + VO_3 \rightarrow O_3, \tag{3d}$$

$$I_{Si} + VO_4 \rightarrow O_4, \tag{3e}$$

where A′ is the constituent of A remaining after the release of I_{Si}.

2. Reactions of oxygen complexes

Inclusion of O_2 in the reaction model has been carried out by considering the measured evolution of $[O_2]$ during annealing and Figure 4 illustrates the gradual development of the implementation. First, we add only the reactions of O_2 with the VO_n species (model A), which is not sufficient to describe the experimental data, since the simulated values of $[O_2]$ remain almost constant. Second, the very likely reactions $O_2 + O_i \rightarrow O_3$ and $O_2 + O_2 \rightarrow O_4$ are accounted for (model B), yielding a too fast decrease of $[O_2]$ compared to the experimental data. The fast decrease is due mainly to the trimer formation, governed by the rate equation $4\pi R(D_{O_2} + D_{O_i})[O_2][O_i]$ and found to be three orders of magnitude larger in rate than any of the other reactions. Thus, a back reaction $O_3 \rightarrow O_2 + O_i$ is included to balance the fast decrease of $[O_2]$, as shown by model C; $[O_2]$ reaches now

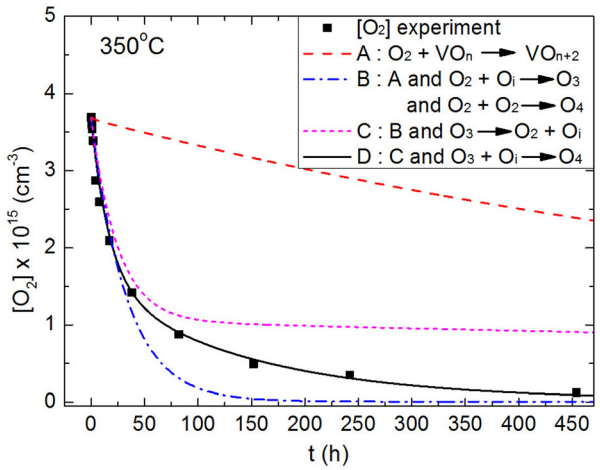

FIG. 4. Comparison between calculated (lines) and experimental (symbols) concentrations of O_2 during isothermal annealing at 350 °C using four different simulation models.

equilibrium rapidly and the model is not able to follow the measured values at times in excess of 50 h. It is well established from previous studies that the formation of O_n defects cannot be explained by one fast diffusing species only and O_3 is predicted to be a faster diffuser than O_i.[29] Hence, O_3 is not the "final" defect but reacts with O_i to form higher order complexes, and in model D also the reaction $O_3 + O_i \rightarrow O_4$ is included. In fact, evidence for O_3 and a development with annealing time can be found in the spectra for the hot-irradiated samples (Fig. 1(b)), and it actually occurs already prior to any annealing with a LVM located at $1005\,cm^{-1}$ on the tail of the prominent O_2 band. Accordingly, the hot irradiation does not only give rise to excess of $[O_2]$, primarily via the reaction $VO_2 + I_{Si} \rightarrow O_2$, but also promotes the formation of O_3 through reactions like $VO_3 + I_{Si} \rightarrow O_3$ and $O_2 + O_i \rightarrow O_3$. Averaging for all the samples, it appears that $[O_2]_{t=0} = 2 \times [VO_2]_{t=0}$ after hot irradiation and a corresponding relation seems also to hold for O_3, i.e., $[O_3]_{t=0} = 2 \times [VO_3]_{t=0}$, although with a higher uncertainty than for O_2. Model D displays a good agreement with the experimental values of $[O_2]$ and in the "complete" model, the following reactions (4a)–(4f) are included:

$$O_i + O_i \rightarrow O_2, \tag{4a}$$

$$O_2 + O_i \rightarrow O_3, \tag{4b}$$

$$O_2 + O_2 \rightarrow O_4, \tag{4c}$$

$$O_3 + O_i \rightarrow O_4, \tag{4d}$$

$$O_2 \rightarrow O_i + O_i, \tag{4e}$$

$$O_3 \rightarrow O_2 + O_i. \tag{4f}$$

C. Quantitative comparison between experimental data and simulation results

On the basis of the reactions described above (Eqs. (1a)–(1h), (2a)–(2g), (3a)–(3e), and (4a)–(4f)), the corresponding coupled differential equations derived from the theory for diffusion limited reactions are given in Table I and they have been numerically solved using Matlab. In the simulations, the diffusivity of O_i has been taken from the literature,[13] while the diffusivity and dissociation rates of O_2, O_3 VO, VO_2, VO_3, and VO_4 have been used as fitting parameters. For the RT-irradiated samples, the initial concentrations of O_i and VO were taken from the peak amplitude of their corresponding LVMs, and all the other defect concentrations were initialized to zero. For the hot-irradiated samples, the initial concentration of O_i, O_2, VO, VO_2, VO_3, and VO_4 were taken from the peak amplitude of their corresponding LVMs. The initial concentrations of O_3 and A have been taken as $[O_3]_{t=0} = 2 \times [VO_3]_{t=0}$ and $[A]_{t=0} = 0.1 \times [O_2]_{t=0}$. Here, it should be noted that the model exhibits good stability where the input values of the defect concentrations can be varied over many orders of magnitude and yield stable solutions.

TABLE I. Rate equations derived from Eqs. (1a)–(1h), (2a)–(2g), (3a)–(3e), and (4a)–(4f).

Defect	Rate equation
O_i	$\frac{d[O_i]}{dt} = 4\pi R\{D_{I_{Si}}[I_{Si}][VO] - 2D_{O_i}[O_i]^2 - D_{O_2}[O_i][O_2] - D_{O_3}[O_i][O_3] - D_{VO}[O_i][VO] - D_{VO_2}[O_i][VO_2] - D_{VO_3}[O_i][VO_3] - D_{O_i}[O_i][VO_4]\}$ $+2C^{diss}_{O_2}[O_2] + C^{diss}_{O_3}[O_3] + C^{diss}_{VO}[VO] + C^{diss}_{VO_2}[VO_2] + C^{diss}_{VO_3}[VO_3] + C^{diss}_{VO_5}[VO_5]$
O_2	$\frac{d[O_2]}{dt} = 4\pi R\{D_{O_i}[O_i]^2 + D_{I_{Si}}[I_{Si}][VO_2] - D_{O_2}[O_i][O_2] - 2D_{O_2}[O_2]^2 - (D_{VO} + D_{O_2})[VO][O_2] - (D_{VO_2} + D_{O_2})[VO_2][O_2]$ $-(D_{VO_3} + D_{O_2})[O_2][VO_3] - D_{O_2}[VO_4][O_2]\} - C^{diss}_{O_2}[O_2] + C^{diss}_{O_3}[O_3] + C^{diss}_{VO_5}[VO_5] + C^{diss}_{VO_6}[VO_6]$
O_3	$\frac{d[O_3]}{dt} = 4\pi R\{D_{O_2}[O_i][O_2] + D_{I_{Si}}[I_{Si}][VO_3] - D_{O_3}[O_i][O_3]\} - C^{diss}_{O_3}[O_3]$
VO	$\frac{d[VO]}{dt} = 4\pi R\{-D_{VO}[O_i][VO] - (D_{VO} + D_{O_2})[VO][O_2] - D_{I_{Si}}[I_{Si}][VO]\} - C^{diss}_{VO}[VO] + C^{diss}_{VO_2}[VO_2]$
VO_2	$\frac{d[VO_2]}{dt} = 4\pi R\{D_{VO}[O_i][VO] - D_{VO_2}[O_i][VO_2] - (D_{VO_2} + D_{O_2})[VO_2][O_2] - D_{I_{Si}}[I_{Si}][VO_2]\} - C^{diss}_{VO_2}[VO_2] + C^{diss}_{VO_3}[VO_3]$
VO_3	$\frac{d[VO_3]}{dt} = 4\pi R\{D_{VO_2}[O_i][VO_2] + (D_{VO} + D_{O_2})[VO][O_2] - D_{VO_3}[O_i][VO_3] - (D_{VO_3} + D_{O_2})[O_2][VO_3] - D_{I_{Si}}[I_{Si}][VO_3]\} - C^{diss}_{VO_3}[VO_3]$
VO_4	$\frac{d[VO_4]}{dt} = 4\pi R\{D_{VO_3}[O_i][VO_3] + (D_{VO_2} + D_{O_2})[VO_2][O_2] - D_{O_i}[O_i][VO_4] - D_{O_2}[VO_4][O_2] - D_{I_{Si}}[I_{Si}][VO_4]\} - C^{diss}_{VO_4}[VO_4]$
I_{Si}	$\frac{d[I_{Si}]}{dt} = C^{diss}_{A}[A] - 4\pi R\{D_{I_{Si}}[I_{Si}][VO] - D_{I_{Si}}[I_{Si}][VO_2] - D_{I_{Si}}[I_{Si}][VO_3] - D_{I_{Si}}[I_{Si}][VO_4]\}$

The simulation results are compared with the experimental data in Figs. 5 and 6 for the RT-irradiated and hot-irradiated samples, respectively. The experimental data represent results from 14 different samples isothermally annealed in the 300 °C–500 °C temperature range, and for all samples, irrespective of RT- or hot-irradiation, a good quantitative agreement is demonstrated between the experiments and the simulation results for O_i, O_2, and VO_n ($n \leq 4$).

For the RT-irradiated samples, the transformation of VO into VO_2 through diffusion and trapping by O_i is well described by the model, in accordance with previous results in the literature.[5,15] In particular, at 350 °C and 370 °C, the transformation can be followed in detail during the initial stages while at higher temperatures, it occurs rapidly and already within the first annealing duration. The subsequent decrease of $[VO_2]$ correlates closely with the increase in $[VO_3]$ for all the temperatures studied. Here, it can be emphasized that the present model is more complete than the one assumed previously in Ref. 20 and no defect X, of unknown origin, needs to be introduced to explain the evolution of VO_3 at temperatures above 450 °C.

For the hot-irradiated samples (Fig. 6), it is demonstrated that O_2 plays a significant role in the evolution of the VO_n species (cf. also Fig. 3(b)) although the reverse effect, i.e., the influence of VO_n on the evolution of O_2, is weak (cf. also Fig. 4). In fact, the decrease of $[O_2]$ with annealing time is mainly due to the formation of higher order oxygen complexes (O_3 and O_4) and not to interaction with VO_4. Further, an important outcome is that O_3 is a fast diffusing species with a diffusivity similar to that of O_2, and O_3 can also dissociate into O_2 and O_i. These properties of O_3 are in full accordance with the results from density-functional-theory

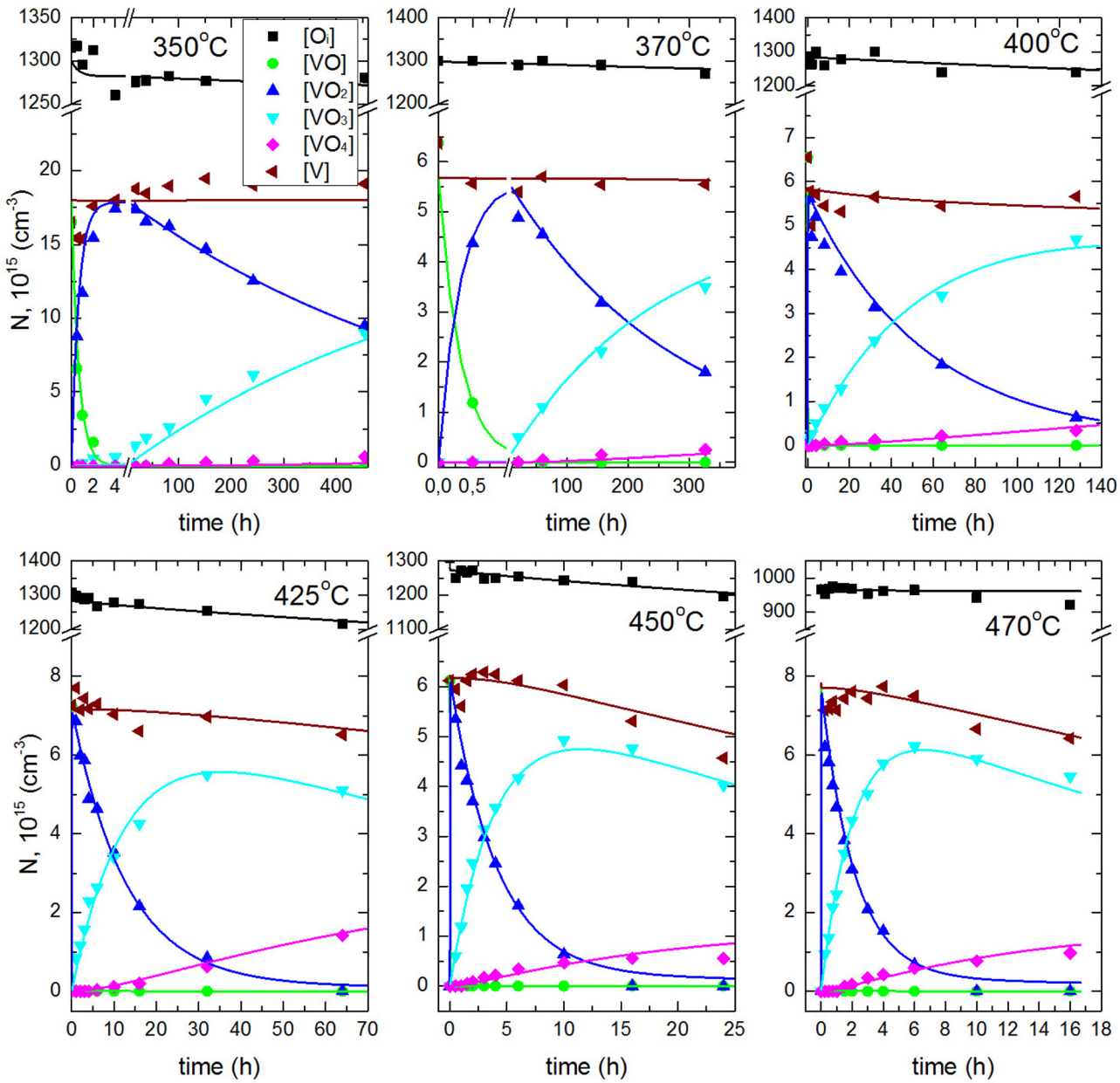

FIG. 5. Comparison between simulated (lines) and experimental (symbols) concentrations of O_n and VO_n versus time during isothermal annealing at different temperatures for samples irradiated at room temperature.

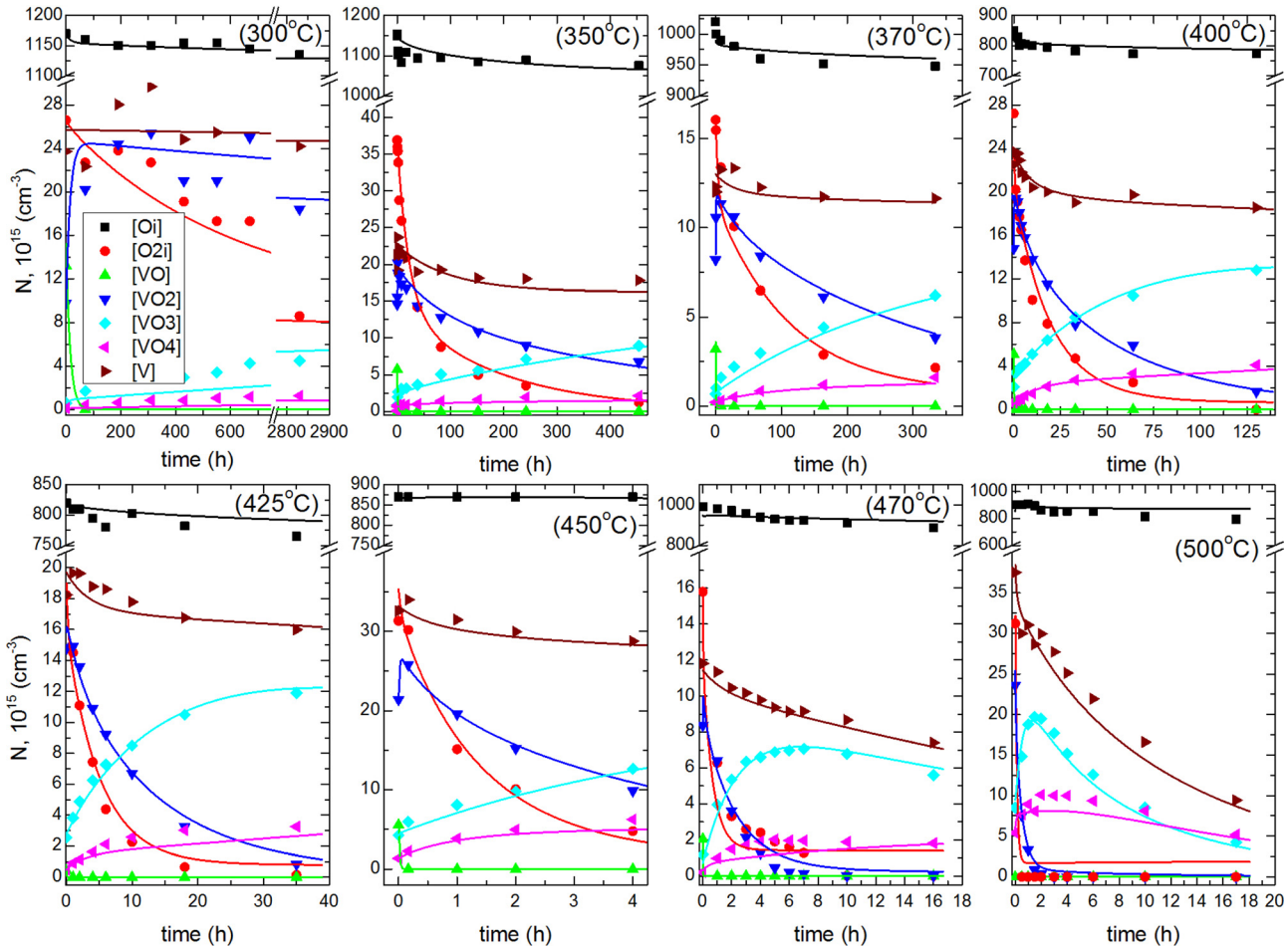

FIG. 6. Comparison between simulated (lines) and experimental (symbols) concentrations of O_n and VO_n versus time during isothermal annealing at different temperatures for samples irradiated at 350 °C.

calculations predicting that O_3 plays a key role in the formation of oxygen related thermal donors.[30,31] Here, it should be noted that for long annealing times at the two highest temperatures used (470 °C and 500 °C), thermal donor formation is pronounced and for these annealing conditions we observe a deviation of about $\sim 2 \times 10^{15}\,cm^{-3}$ between the experimental and simulated data for $[O_2]$; the simulations predict an equilibrium value while experimentally $[O_2]$ decreases below the detection limit. Considering the excellent agreement between experiment and modeling for shorter times at 470 °C and 500 °C and in all the other cases of annealing temperatures and durations studied, this deviation is regarded as significant albeit being rather small in absolute values. The main cause of the predicted $[O_2]$ equilibrium is due to a steady-state between the forward and backward rates of the reaction $O_i + O_i \rightleftharpoons O_2$. The forward one increases strongly at high temperatures because of the high activation energy of D_{O_i} ($E_a \sim 2.5$ eV) and this cannot be balanced by a corresponding increase of the dissociation rate since then the model fails shorter times and at all the other annealing temperatures and times studied. In this context, we also considered the effect of the cooling rate after annealing (~100 °C/min) where the forward reaction ceases more rapidly than the backward one because of a higher E_a. However, this cannot account for more than ~25% of the observed deviation and a more likely explanation is that O_2 reacts with O_3 and O_4 forming higher order complexes possibly related to thermal donors.[30,31] Such reactions reduce the steady-state-concentration of O_2 at higher temperature/long times especially since both O_2 and O_3 are quite mobile and possibly even O_4.[30,31] Unfortunately, experimental evidence for these reactions is scarce in the literature and therefore, they have not been included in the model. Hence, further experiments to monitor the detailed kinetics of the O_3 evolution are encouraged utilizing the novel concept of defect engineering by hot irradiation, outlined in Ref. 14, to prepare samples with a desirable initial concentration of O_3.

Similarly, further studies need to be pursued regarding the origin of the A (and A′) center, which is presently not known. However, the A center involves I_{Si} and is promoted by irradiation at 350 °C. At this elevated irradiation temperature, the role of substitutional C_s atoms as competing traps for migrating I'_{Si}s ($I_{Si} + C_s \rightarrow C_i$) is suppressed relative to that at RT because of a low thermal stability of the resulting complexes formed by C_i.[24] Accordingly, the back reaction of C_i to I_{Si} and C_s becomes very likely and the probability of forming high-order and stable intrinsic clusters of I'_{Si}s is expected to increase during the 350 °C irradiation. A very tentative and speculative identification of A is the stable cluster of four I'_{Si}s ($(I_{Si})^4$), discussed by Cowern *et al.*[32]

Figure 7 shows the diffusivity and dissociation rate values deduced from the simulations versus 1/kT, and it should be emphasized that these values are valid for both batches of the samples (RT-irradiated and hot-irradiated). Indeed, this strongly strengthens the consistency and validity of the results. The values exhibit Arrhenius behavior and the activation energies and the exponential prefactors related to the migration and the dissociation rates of the different defects are summarized in Table II. For instance, the values for VO are in good agreement with those reported previously in the literature.[15–17] Further, the diffusivity of VO_n decreases with increasing n, primarily via an increasing migration barrier but also because of a slight decrease in the prefactor. This supports the assumption that VO_4 is less mobile than the smaller species and do not contribute significantly to the formation of VO_5 and VO_6. With a possible exception for VO_4, the dissociation rates of VO_n in Fig. 7(b) reveal a decreasing tendency with n, in spite of $E_a^{dissociation}$ remaining constant at 2.55 eV (Table II). This suggests that the effective barrier for dissociation is the same for the different VO_n defects and it is interesting to note that the value of 2.55 eV is practically identical with the activation energy of O_i diffusion.[13] Hence, it may be argued that the rate limiting process during dissociation is due to the Si-O-Si bond breaking when the O atom diffuses away from (or is released from) the remaining VO_{n-1} defect. Further, the decrease in K, or more precisely k_0, with increasing defect size arises then from an increasing probability of re-capture of the O-atom just attempting to be released. Especially, the reduction in k_0 is large between VO and VO_2 (slightly more than one order of magnitude) reflecting a lower thermal stability of a dissociated $V + O_i$ atomic configuration than that of a $VO + O_i$ configuration and hence a lower probability of re-capture. In fact, the $VO + O_i$ configuration has been reported in the literature and is denoted as the VO_2^* defect.[27] Between VO_2 and VO_3, the decrease in k_0 is only a factor of ~2 consistent with more similar dissociated configurations of these two defects (VO_2^* versus $VO_2 + O_i$). For VO_4, the accuracy of the deduced K values is lower than that for VO, VO_2 and VO_3, and no comparison of k_0 can be made with confidence. However, the general trend of the data corroborates an increasing stability of VO_n with size and supports the assumption made in the simulations regarding a high stability of VO_5 and VO_6 in the studied temperature range. In this context, it should also be underlined that the k_0 values obtained for VO_n ($n \leq 4$) are all in the 10^{12}–$10^{13} s^{-1}$ range, as expected for dissociative processes.[33]

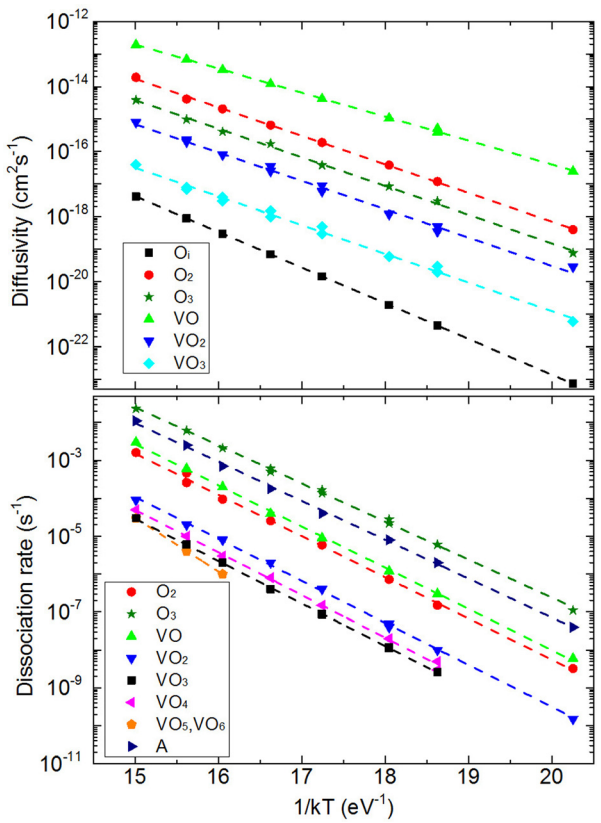

FIG. 7. Arrhenius plot of the (a) diffusion and (b) dissociation rates extracted from the simulation.

TABLE II. Activation energies and prefactors of diffusivity and dissociation constants extracted from their corresponding Arrhenius plots. The values for O_i are taken from Ref. 13. The errors represent the standard deviation of the linear fitting.

Diffusivity (D)		
Defects	E_a (eV)	d_0 ($cm^2 s^{-1}$)
O_i	2.53 ± 0.01	0.125 ± 0.005
O_2	2.02 ± 0.01	0.264 ± 0.030
O_3	2.00 ± 0.01	0.065 ± 0.020
VO	1.71 ± 0.01	0.026 ± 0.001
VO_2	1.99 ± 0.03	0.005 ± 0.008
VO_3	2.04 ± 0.04	0.001 ± 0.002
Dissociation constants (K)		
Defects	E_a (eV)	k_0 (s^{-1})
O_2	2.52 ± 0.03	$(3.1 \pm 0.3) \times 10^{13}$
O_3	2.33 ± 0.03	$(2.9 \pm 0.5) \times 10^{13}$
VO	2.55 ± 0.02	$(5.6 \pm 0.7) \times 10^{13}$
VO_2	2.53 ± 0.02	$(4.7 \pm 0.8) \times 10^{12}$
VO_3	2.55 ± 0.03	$(1.4 \pm 0.8) \times 10^{12}$
VO_4	2.59 ± 0.03	$(3.8 \pm 0.7) \times 10^{12}$
A	2.36 ± 0.04	$(2.4 \pm 0.8) \times 10^{13}$

In accordance with theoretical predictions,[30,31] O_2 and O_3 are found to be fast diffusers relative to O_i (Fig. 7(a)). Both species exhibit a migration barrier of ~2.0 eV but d_0 is about a factor of 4 higher for O_2, which may indicate more correlated jumps of the two constituents in the dimer, leading to migration, than that of the three ones in the trimer. Further, the dissociation barrier of O_3 is ~0.2 eV lower than that of O_2 implying a weaker bonding of the third O-atom in O_3 and thus challenging theoretical results suggesting similar thermal stability of O_3 and O_2.[34,35]

A comparison of the barrier values for migration and dissociation in Table II yields a difference ($E_a^{dissociation} - E_a^{migration}$) of ~0.3 eV for O_3, ~0.8 eV for VO, and ~0.5 eV for the other defects. Thus, in all cases, $E_a^{dissociation} > E_a^{migration}$ clearly indicating that partial dissociation prevails during the migration processes of all the different defects. Finally, the Arrhenius plot

in Fig. 7(a) provides a compelling compilation of data showing that interstitial oxygen is the slowest diffuser and substitutional oxygen, i.e., VO, is the fastest one with a difference of ~7 to ~4 orders of magnitude in the studied temperature range. The diffusivities of all the other defects are in between those of O_i and VO, and it shows conclusively that excess vacancies, dimers, and trimers strongly promote the transport of oxygen in silicon.

IV. CONCLUSION

A comprehensive experimental study of the evolution of the O_i, O_2, and VO_n ($n \leq 4$) defects during isothermal annealing of RT-irradiated and hot-irradiated Cz-Si samples has been carried out at temperatures between 300 and 500 °C. Despite quite different initial conditions prior to the annealing, the defect kinetics in both sets of samples is shown to be quantitatively described by the same reaction model and the same values of defect diffusivities and dissociation rates. This supports, indeed, the validity of the model, which assumes a sequential build-up of the VO_n defects. Values for the activation energies and exponential prefactors of the diffusivities and dissociation rates of VO_n, O_2, and O_3 have been deduced and in general, the mobility and stability of VO_n decrease and increase with n, respectively. For all the defects, partial dissociation appears to be a prevailing mechanism during diffusion, while the Si–O–Si bond breaking of similar kind as for O_i diffusion seems to limit the dissociation of the VO_n defects, which all display a value of ~2.55 eV for $E_a^{dissociation}$. Both O_2 and O_3 are fast diffusers with $E_a^{migration} \approx 2.0$ eV, whilst the thermal stability of O_3 is found to be substantially lower than that of O_2, challenging theoretical predictions in the literature.

ACKNOWLEDGMENTS

Numerous and enlightening discussions with Professor J. L. Lindström on the subject of oxygen in silicon are gratefully acknowledged as well as experimental assistance during the initial stage of the study. The work was supported by the Norwegian Research Council, Industry partners and Research partners through the Norwegian Research Centre for Solar Cell Technology (FME-SOL). L. I. Murin thanks Fund for Fundamental Research of the Republic of Belarus (Grant No. T14-040) for a partial financial support.

[1]A. Borghesi, B. Pivac, A. Sassella, and A. Stella, J. Appl. Phys. **77**, 4169 (1995).
[2]S. W. Glunz, S. Rein, J. Y. Lee, and W. Warta, J. Appl. Phys. **90**, 2397 (2001).
[3]K. Bothe and J. Schmidt, J. Appl. Phys. **99**, 013701 (2006).
[4]L. Chen, X. Yu, P. Chen, P. Wang, X. Gu, J. Lu, and D. Yang, Sol. Energy Mater. Sol. Cells **95**, 3148 (2011).
[5]J. W. Corbett, D. Watkins, and R. S. McDonald, Phys. Rev. **135**, A1381 (1964).
[6]J. L. Lindström and B. G. Svensson, *Oxygen, Carbon, Hydrogen and Nitrogen in Crystalline Silicon* (Mater. Res. Soc. Symp. Proc., 1986), Vol. 59, p. 45.
[7]C. A. Londos, L. G. Fytros, and G. J. Georgiou, Defect Diffus. Forum **171–172**, 1–32 (1999).
[8]V. V. Voronkov and R. Falster, J. Electrochem. Soc. **149**(3), G167–G174 (2002).
[9]T. Hallberg, J. L. Lindström, L. I. Murin, and V. P. Markevich, Mater. Sci. Forum **258–263**, 361–366 (1997).
[10]D. Åberg, B. G. Svensson, T. Hallberg, and L. Lindström, Phys. Rev. B **58**, 12944 (1998).
[11]L. I. Murin, T. Hallberg, V. P. Markevich, and J. L. Lindström, Phys. Rev. Lett. **80**, 93–96 (1998).
[12]J. L. Lindström, T. Hallberg, J. Hermansson, L. I. Murin, V. P. Markevich, M. Kleverman, and B. G. Svensson, Solid State Phenom. **69–70**, 297 (1999).
[13]R. C. Newman, J. Phys.: Condens. Matter **12**, R335–R365 (2000).
[14]L. I. Murin, E. A. Tolkacheva, V. P. Markevich, A. R. Peaker, B. G. Svensson, and J. L. Lindström, Phys. Status Solidi C **8**, 709–712 (2011).
[15]B. G. Svensson and J. L. Lindström, Phys. Rev. B **34**, 8709 (1986).
[16]M. Mikelsen, J. H. Bleka, J. S. Christensen, E. V. Monakhov, B. G. Svensson, J. Harkönen, and B. S. Avset, Phys. Rev. B **75**, 155202 (2007).
[17]V. V. Voronkov, R. Falster, and C. A. Londos, J. Appl. Phys. **111**, 113530 (2012).
[18]J. L. Lindström, L. I. Murin, T. Hallberg, V. P. Markevich, B. G. Svensson, M. Kleverman, and J. Hermansson, Nucl. Instrum. Methods Phys. Rev. B **186**, 121–125 (2002).
[19]L. I. Murin, J. L. Lindström, B. G. Svensson, V. P. Markevich, A. R. Peaker, and C. A. Londos, Solid State Phenom. **108–109**, 267–272 (2005).
[20]V. Quemener, B. Raeissi, F. Herklotz, L. I. Murin, E. V. Monakhov, and B. G. Svensson, Phys. Status Solidi B **251**, 2197–2200 (2014).
[21]L. I. Murin and B. G. Svensson, unpublished results.
[22]S. Öberg, C. P. Ewels, R. Jones, T. Hallberg, J. L. Lindström, L. I. Murin, and P. R. Briddon, Phys. Rev. Lett. **81**, 2930 (1998).
[23]T. R. Waite, Phys. Rev. **107**, 463–470 (1957).
[24]E. V. Monakhov and B. G. Svensson, *Silicon, Germanium and Their Alloys: Growth, Defects, Impurities and Nanocrystals*, edited by G. Kissinger and S. Pizzini (CRC Press, 2014).
[25]H. J. Stein, Appl. Phys. Lett. **48**, 1540 (1986).
[26]G. G. DeLeo, C. S. Milsted, Jr., and J. C. Kralik, Phys. Rev. B **31**, 3588 (1985).
[27]J. L. Lindström, L. I. Murin, B. G. Svensson, V. P. Markevich, and T. Hallberg, Physica B **340–342**, 509–513 (2003).
[28]G. Davies and R. C. Newman, *Carbon in Monocrystalline Silicon: Handbook on Semiconductors* (Elsevier, 1994), Vol. 3.
[29]L. I. Murin and V. P. Markevich, *Early Stage of Oxygen Precipitation in Silicon* (Kluwer Academic, Dordrecht, The Netherlands, 1996).
[30]Y. J. Lee, J. von Boehm, M. Pesola, and R. M. Nieminen, Phys. Rev. Lett. **86**, 3060–3063 (2001).
[31]Y. J. Lee, J. von Boehm, and R. M. Nieminen, Phys. Rev. B **66**, 165221 (2002).
[32]N. E. B. Cowern, G. Mannino, P. Stolk, F. Roozeboom, H. G. A. Huizing, G. M. van Berkum, F. Cristiano, A. Claverie, and M. Jaraiz, Phys. Rev. Lett. **82**, 4460 (1999).
[33]J. W. Corbett, *Electron-Radiation Damage in Semiconductors and Metals*, edited by F. Seitz and D. Turnbull (Academic, New York, 1966).
[34]D. J. Chadi, Phys. Rev. Lett. **77**, 861 (1996).
[35]M. Pesola, J. von Boehm, T. Mattila, and R. M. Nieminen, Phys. Rev. B **60**, 11449 (1999).